JOURNAL OF AIRCRAFT
Vol. 45, No. 6, November–December 2008

Active Flow Control on a Nonslender Delta Wing

N. M. Williams,* Z. Wang,† and I. Gursul‡
University of Bath, Bath, England BA2 7AY, United Kingdom

DOI: 10.2514/1.37486

The effects of active flow control by oscillatory blowing at the leading edge of a nonslender delta wing with a 50-degree sweep angle have been investigated. Pressure measurements and particle image velocimetry measurements were conducted to investigate the formation of leading-edge vortices for oscillatory blowing, compared with completely stalled flow for the no-blowing case. Stall has been delayed substantially and significant increases in the upper surface suction force have been observed. For a given angle of attack, there is an optimal momentum coefficient, after which forcing at higher momentum coefficients has negligible effect. For the poststall region, as the angle of attack increases, the optimal momentum coefficient increases. Velocity measurements show that the flow reattachment is promoted with forcing, and a vortex flow pattern develops. The time-averaged location of the center of the vortical region moves outboard with excitation. The near-surface flow pattern obtained from the particle image velocimetry measurements shows the reattachment clearly in the forward part of the wing. There is no jetlike axial flow in the core of the vortex, which seems to have breakdown at or very near the apex. Phase-averaged measurements reveal the perturbation due to the pulsed blowing, its interaction with the shear layer and vortex, apparent displacement of the vortex core, and relaxation of the reattachment region. Experiments with excitation from finite span slots located in the forward half of the wing show that partial blowing may be more effective at low momentum coefficients and promote reattachment upstream of the slot.

Nomenclature

A_{jet}	=	cross-sectional area of the jet slot
C_p	=	pressure coefficient
C_S	=	suction force coefficient
C_μ	=	momentum coefficient
c	=	wing chord
E	=	effectiveness, $\Delta C_S/C_\mu$
f	=	pulsing frequency
S	=	wing area
St	=	Strouhal number, fc/U_∞
s	=	semispan
U_{jet}	=	jet velocity at the slot exit
U_∞	=	wind-tunnel freestream velocity
x	=	chordwise distance
y	=	spanwise distance
z	=	distance from the wing surface in a plane normal to the freestream
α	=	angle of attack

I. Introduction

NONSLENDER delta wings (with sweep angles between 35 and 55 deg) have various applications. These range from military fighter aircraft to civilian surveillance micro air vehicles. With the growing interest in micro air vehicles and unmanned air vehicles, the aerodynamics of nonslender delta wings and flow control aspects need to be investigated. Active flow control can enhance the lift at high angles of attack. In particular, active flow control may help to extend the boundaries of low-Reynolds-number flight. This paper focuses on the active control of flow over nonslender delta wings by oscillatory blowing from the leading edge.

It is known that the unsteady excitation has little effect on vortex breakdown [1] but can excite the Kelvin–Helmholtz instability of the separated shear layer and promote reattachment. One of the distinct features of nonslender wings is that the primary attachment line occurs on the surface outboard of the symmetry plane, even when vortex breakdown is near the apex. In contrast, for highly swept wings, reattachment on the wing surface does not occur beyond very small angles of attack, and therefore is difficult to manipulate [1]. For nonslender wings, reattachment of the flow on the wing surface can be manipulated. In particular, active and passive control of reattachment becomes possible in the poststall region, which is the main focus of this paper.

For nonslender delta wings, the motivation for active flow control by unsteady excitation originated from recent studies on oscillating wings and flexible wings [2–8], which reported two effects in the poststall regime. First, reattachment of the separated shear layer is observed, as shown in Fig. 1a. This is similar to the effect of excitation on flow over a backward-facing step [9]. Second, with increasing excitation frequency and amplitude, leading-edge vortices develop with axial flow in the cores, as shown in Fig. 1b, called vortex reformation. For an oscillating wing with a 38.7 deg sweep angle in the poststall regime, it was shown [2] that there is a recovery of the topological features of a leading-edge vortex in the crossflow plane relative to those on the stationary wing. Experiments on an oscillating delta wing with a 50 deg sweep angle [3,4] demonstrated the reattachment of the otherwise stalled flow. In extensive studies for various sweep angles [5], the effects of forcing frequency, amplitude, wing sweep angle, and spatial mode of excitation were investigated. Totally separated flow for the stationary wing at poststall incidences becomes reattached to the wing surface for the oscillating wing. Flow visualization and particle image velocimetry (PIV) measurements indicate that reattachment starts very close to the apex when the frequency of the perturbations is in a certain range.

Recent studies of flexible nonslender wings ($\Lambda = 40$ to 55 deg) reported lift enhancement in the poststall region [6–8] (see Fig. 2a). This lift enhancement was associated with self-excited wing vibrations in the poststall region. These vibrations took place in an antisymmetric structural mode and promoted reattachment of the separated shear layer to the wing surface (Fig. 2b). The structure of the reattached flow was found to be similar to a three-dimensional

Presented as Paper 740 at the 46th AIAA Aerospace Sciences Meeting and Exhibit, Reno, NV, 7–10 January 2008; received 11 March 2008; revision received 17 June 2008; accepted for publication 17 June 2008.

*Ph.D. Student, Department of Mechanical Engineering. Student Member AIAA.
†Research Councils United Kingdom Academic Fellow, Department of Mechanical Engineering.
‡Professor, Department of Mechanical Engineering. Associate Fellow AIAA.

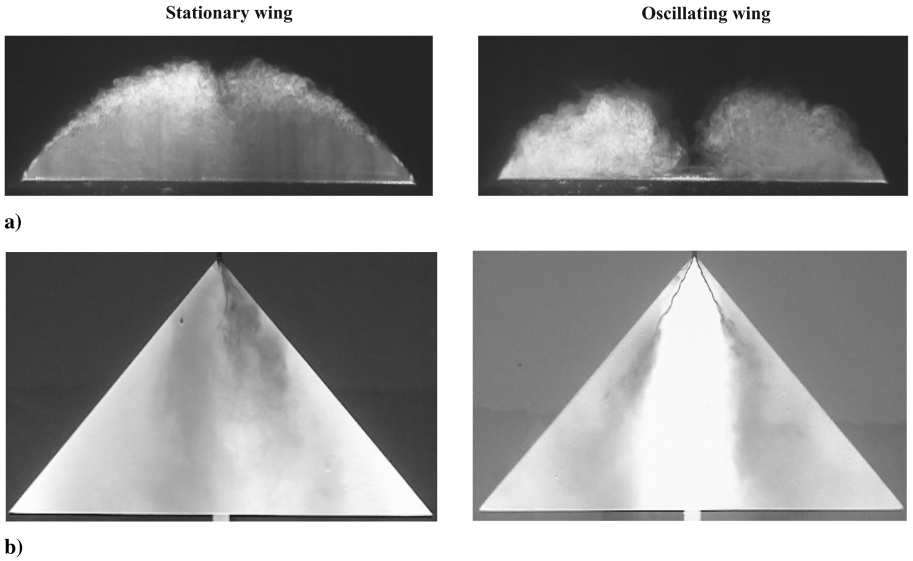

Fig. 1 Flow visualization of a) reattachment in a crossflow plane and b) vortex reformation [5].

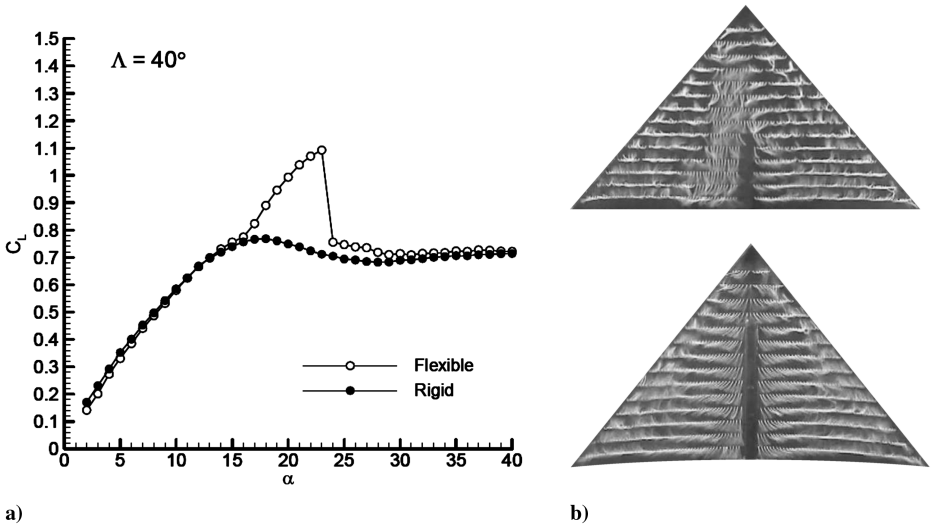

Fig. 2 Comparison of a) lift coefficient and b) tuft flow visualization for rigid (upper) and flexible (lower) delta wings [8].

conical separation bubble in the time-averaged sense. For both oscillating rigid wings and flexible vibrating wings, an interesting observation was the development of a leading-edge vortex with axial flow (and subsequent breakdown further downstream) when the excitation amplitude was sufficient and the frequency was in an optimum range.

The reattachment process with excitation is generic for nonslender wings and there is an optimum frequency range of $fc/U_\infty = 1$ to 2. Measurements of both the location of reattachment and location of vortex breakdown indicate the existence of an optimum range of frequencies, which is believed to be related to the dominant frequencies of the shear-layer instabilities [10,11]. For example, vortex breakdown is delayed to a maximum distance from the apex for this range of frequencies. The Strouhal number of the dominant frequency of the structural vibrations was near unity for all flexible wings [6–8]. Yaniktepe and Rockwell [2] suggested that the most effective frequency of excitation ($fc/U_\infty = 2.06$) corresponded to the subharmonic of the dominant frequency in the region of the shear layer closest to the leading edge at $x/c = 0.8$. A similar suggestion was previously made by Gad-el-Hak and Blackwelder [12] for a sweep angle of 60 deg. However, the shear-layer instabilities are three-dimensional and the dominant frequency decreases in the streamwise direction [8]. Hence, multiple time scales exist for the three-dimensional separated flow over a delta wing in the poststall regime. Nevertheless, the measurements indicate dominant frequencies in the range of $fc/U_\infty = 1$ to 5 for a stalled wing with $\Lambda = 50$ deg. A similar range of optimum frequencies was reported for a more slender wing [13]. Margalit et al. [13] showed that zero mass-flux excitation at the leading edge can enhance the lift in the poststall region of a delta wing with $\Lambda = 60$ deg, which is a transitional case between the slender and nonslender wings. The most effective frequency was found in the range of $fc/U_\infty = 1$ to 2.

Wing sweep angle is believed to be an important parameter. For a wing with a zero sweep angle and at a high angle of attack in the poststall region, the formation of a stable separation bubble, in which the flow reattaches completely to the wing surface, is not possible. This is due to the lack of vorticity removal in the spanwise direction. It seems that a moderate sweep angle (such as 50 deg) helps the formation of semiclosed separation bubbles; hence, the wing sweep is beneficial in flow reattachment. Therefore, the effectiveness of the flow control is expected to improve for moderate sweep angles. There is a lower limit of sweep angle (less than 30 deg) below which reattachment was not observed for the oscillating wings. On the other hand, Rullan et al. [14] reported that the flow control effectiveness decreased with increasing sweep angle. For a diamond wing with a sweep angle of 42 deg, the authors reported that the flow control was minimal. It is not known whether this unexpected result is due to the type of unsteady excitation (oscillating mini-flap device) used in

their experiments. In the present paper, we show that flow control is highly effective for a delta wing with a sweep angle of 50 deg. Previous studies on oscillating or vibrating wings formed the foundation for the work on the active flow control approach presented in this paper. The purpose of this study is to investigate the potential of producing the same effect by oscillatory blowing that excites the shear layer at the leading edge. We carried out pressure and velocity measurements to study the effect of oscillatory blowing with a pulsed jet.

II. Experimental Setup

Experiments were conducted in the University of Bath open-jet wind tunnel. The tunnel has a 1-m-long test section and a 0.782 m jet exit diameter. The tunnel has a maximum speed of 30 m/s and a freestream turbulence level of 0.1% when run at the velocity range of the current experiments [15]. The tests were conducted at a freestream velocity of 15 m/s, equating to a Reynolds number of 2×10^5 based on the wing chord length of 0.2 m. The schematic of the tunnel and the camera for the PIV measurements are shown in Fig. 3.

A half-wing model was constructed and used for pressure and PIV measurements in the open-jet wind tunnel. For these tests, the half-body wing was mounted on a splitter plate. Pressure taps were positioned at three streamwise stations, corresponding to $x/c = 0.28$ (station A), $x/c = 0.48$ (station B), and $x/c = 0.68$ (station C). A schematic of the wing, including all pressure tap locations, is shown in Fig. 4. Each tap was connected to a Scannivalve, which connected each tap in turn to a Druck STX 2100 Smart/Hart differential pressure transducer, with a range of 0–10 mbar. Samples were taken at 1000 Hz, each tap was measured for 4 s, and 1.5 s was allowed for switching between stations on the Scannivalve.

Experiments were performed predominantly in the poststall region. Oscillatory blowing with a pulsed jet from a slot near the leading edge was used for the unsteady excitation. Various tip and slot geometries shown in Fig. 5 were tested in preliminary experiments. The slot width in these experiments was 1.2 mm (0.6% of the chord length). These initial tests showed that of the four tip

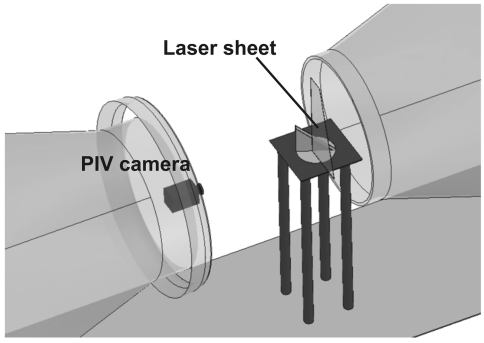

a)

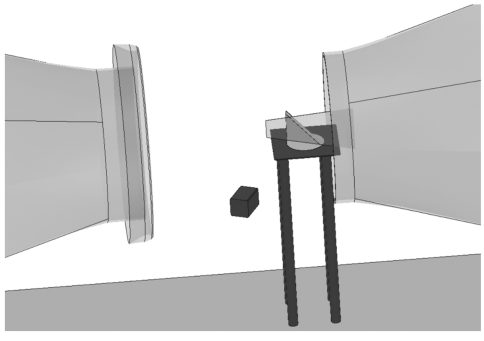

b)

Fig. 3 Experimental setup for half-wing model and schematic of PIV measurements for a) in crossflow plane and b) near-surface velocity measurements.

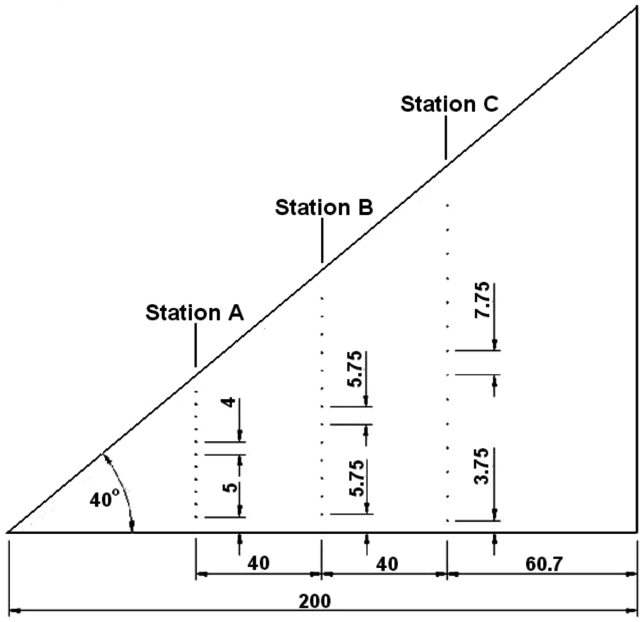

Fig. 4 Plan view of the half-wing model and pressure taps.

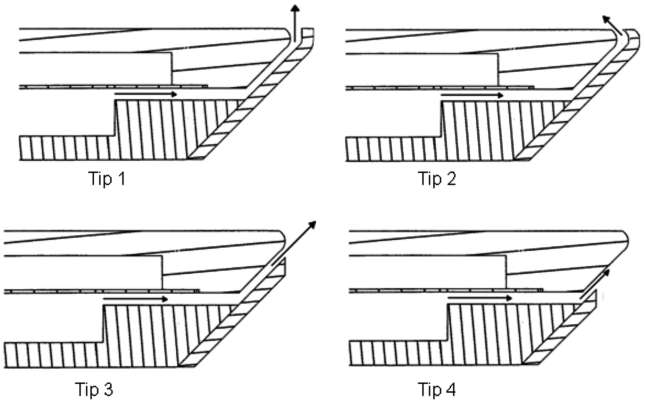

Fig. 5 Cross section of different wing tips tested.

geometries compared, tip 3 consistently gave the greatest increases in suction pressure over the wing, showing the presence of a strong vortexlike pressure profile. On the other hand, tip 4 had almost no effect on the pressure coefficient across the wing. This shows that blowing before the flow separation has no effect. Tip 3 was therefore selected for further investigations presented in this paper.

For oscillatory blowing, an Enfield Tech LS-V15C flow control valve controlled by a LSC-10 controller was used to vary the pulsed-air flow rate with time. The LS-V15C was capable of opening and closing at up to 200 Hz at a high level of repeatability. As the previous investigations showed that the most effective frequencies correspond to $fc/U_\infty = 1$ to 2, the majority of the experiments were conducted for $St = fc/U_\infty = 1.5$. In the preliminary experiments, the effect of the duty cycle was investigated. A short pulse of high-velocity blowing proved to be an effective pulse type. The input signal to the valve was a square wave, and reducing the duty cycle of the input signal to the valve allowed a shorter pulse. An input-signal duty cycle of 20% was chosen because it was the smallest duty cycle that enabled operation across the desired momentum-coefficient range. It was found that there was no real advantage to testing below a 20% duty cycle, as this did not improve the effectiveness of the excitation any further.

The momentum coefficient was controlled by increasing the maximum valve aperture for a given frequency. The momentum-coefficient range tested was from 0 to 1%. The momentum coefficient for each case was found by traversing a Dantec hot-wire probe across the slot at a distance of 3 mm. The traverse was

conducted in 0.1 mm steps, and the length of the traverse depended on the profile of the jet. The overall momentum coefficient was found by integrating across the width of the slot and then over the length of the slot. The uncertainty of the momentum coefficient is estimated to be between 5 and 10%, depending on the frequency and amplitude of the blowing. The greatest uncertainty comes from nonuniform blowing velocity along the slot.

PIV measurements were made to gain a better understanding of the flow dynamics over the wing. A TSI 2-D digital PIV system was used. The PIV system produces pairs of pulses up to 120 mJ focused into a laser sheet at a rate of 3.75 Hz. The PIV camera is a digital charge-coupled device camera with a resolution of 2048×2048 pixels. The seeding for the PIV was provided from a TSI 9306A jet atomizer. Typically, 150–200 pairs of images were taken for each case using an interrogation area of 32×32 pixels. The uncertainty of the velocity measurements is estimated to be 2% of the freestream velocity. Phase-averaged measurements were taken by triggering the PIV system at desired phases of the unsteady excitation. Measurements of velocity in a crossflow plane were taken, as shown in Fig. 3a. The laser sheet was set perpendicularly to the freestream at selected streamwise locations. Measurements were taken at locations corresponding to the location of the pressure tap rows: at $x/c = 0.28$, 0.48, and 0.68. The PIV camera was put into an optical glass box and placed inside the wind tunnel downstream of the delta wing, thus measuring the crossflow velocity field. The effective grid size was around 1.3 mm for these measurements. Vortex-core locations were identified from these crossflow PIV results. The laser sheet was then aligned with the vortex core so that the velocity field in a plane that passes through the vortex core and the apex was measured to obtain the axial velocity in the core. Near-surface measurements were also taken by firing a laser sheet parallel to the wing surface at a distance of 1.5 mm, as shown schematically in Fig. 3b.

III. Results

The effect of pulsed blowing on the time-averaged pressure distribution was investigated in detail. Some examples in the prestall, near-stall, and poststall regimes will be shown here. Based on the previous investigations in a similar Reynolds number range, it is expected that stall is around $\alpha \approx 20$ deg for full-span models. Attar et al. [16] showed by computational simulations for a nonslender delta wing (with a sweep angle of 50 deg) that the onset of stall is delayed for a half-span model, compared with a full-span model. Apparently, imposing the symmetry of the flow at the wing symmetry plane delays the upstream propagation of vortex breakdown and stall. Our pressure data suggest that the stall angle is $\alpha = 23$–24 deg for the half-span model used.

Figure 6 shows the pressure distribution at $x/c = 0.28$ (station A) at $\alpha = 15$, 20, 25, and 30 deg for $St = 1.5$ and various momentum coefficients. For $\alpha = 15$ deg, a well-defined suction peak is observed for the no-control case ($C_\mu = 0$). The effect of pulsed blowing is very small for this incidence. For $\alpha = 20$ deg, the suction peak is nearly the same as that of $\alpha = 15$ deg, and the effect of the vortex is distributed to a larger area for the no-control case. Based on the previous studies for full-span wings, the location of vortex breakdown is expected to be close to the apex. However, for the half-span model, vortex breakdown appears to be delayed. The effect of forcing is a little more pronounced in this case, with the suction peak exceeding $-C_p = 3$. For $\alpha = 25$ and 30 deg, it is seen for $C_\mu = 0$ that

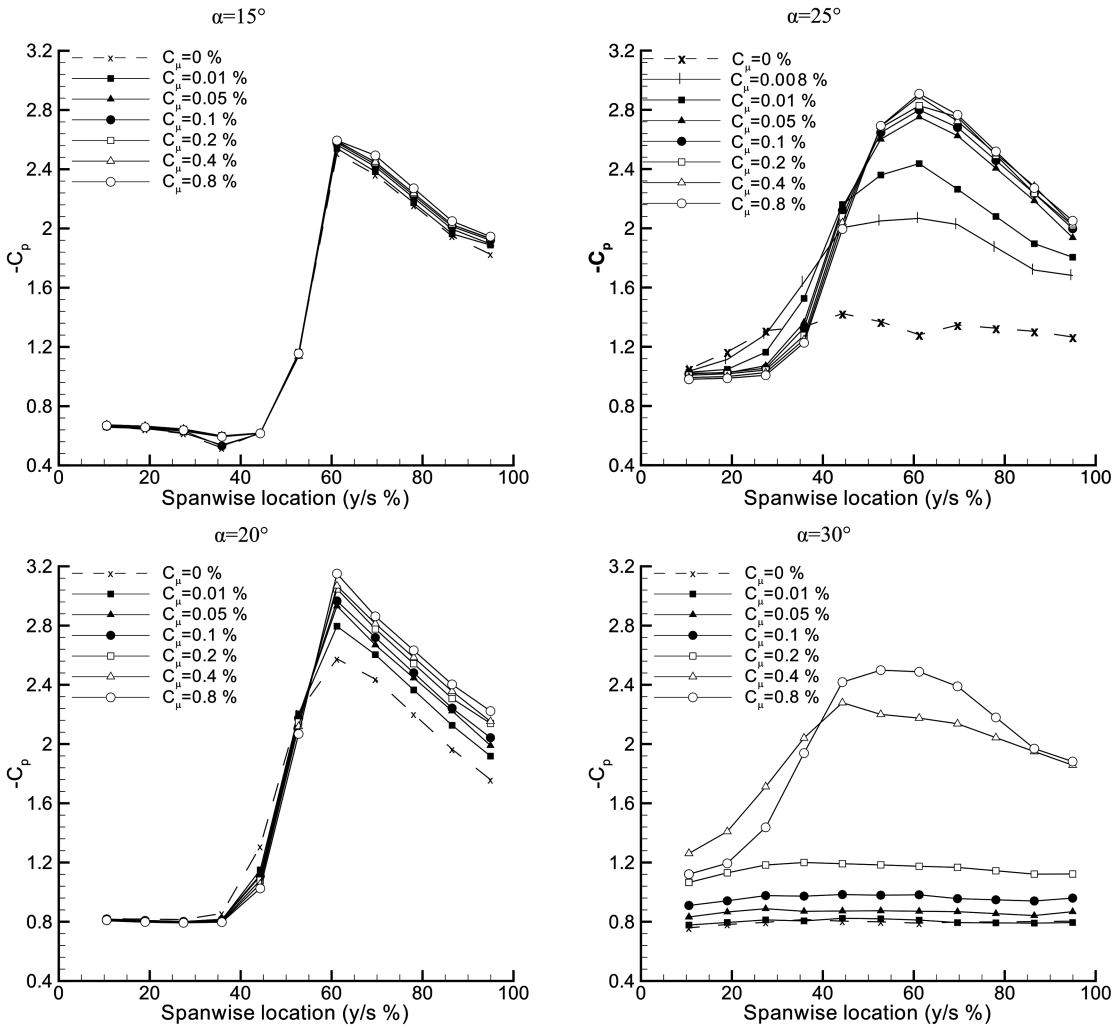

Fig. 6 Spanwise variation of pressure at different angles of attack; $x/c = 0.28$ and $St = 1.5$.

the wing is stalled and has a very flat pressure distribution. In both cases, the introduction of unsteady blowing produces a suction peak and pressure distribution that is characteristic of a leading-edge vortex. As the momentum coefficient increases, a broad vortex pressure distribution initially occurs, indicating a reattachment line close to the wing centerline, as seen for $C_\mu = 0.01\%$ at $\alpha = 25$ deg and $C_\mu = 0.4\%$ at $\alpha = 30$ deg in Fig. 6. For $\alpha = 25$ deg, as the momentum coefficient increases further, the pressure distribution reaches a limit in which both the maximum suction peak and the shape of the pressure distribution are no longer affected by an increase in C_μ. The flow response at this point becomes saturated, indicating that the reattachment process is complete. This occurs at $C_\mu = 0.05\%$ for a 25 deg angle of attack. It is evident that increasing C_μ causes reattachment and that after initial reattachment occurs, increasing C_μ causes the reattachment line to move outboard, forming a tighter vortexlike pressure distribution. For $\alpha = 25$ deg, even very small momentum coefficients are able to produce pressure distribution that is characteristic of a vortex, whereas this happens for much larger momentum coefficients for $\alpha = 30$ deg.

As shown previously, the introduction of pulsing has a strong influence on the pressure across the suction surface in the poststall region. For the purpose of demonstrating the effect of flow control, the pressure distribution at these streamwise stations of the wing ($x/c = 0.28$, 0.48, and 0.68) has been integrated across the span to obtain a sectional suction-force coefficient and then over the surface of the wing to give a suction-force coefficient. This is only an indication of the normal-force coefficient but is sufficient for comparative purposes. The estimated suction-force coefficient C_S is shown in Fig. 7 as a function of angle of attack for $St = 1.5$. In Fig. 7, it is clear that even pulsing with momentum coefficients as low as 0.01% can have a significant effect on the suction force produced. The maximum force coefficient has been increased from 1.05 at 24 deg for $C_\mu = 0$ to 1.23 at 30 deg for $C_\mu = 0.4\%$. This equates to a 17% increase in maximum suction-force coefficient. Stall can also be delayed by up to 8 deg in the case of pulsing at $C_\mu = 0.8\%$. For C_μ values of 0.01% and above, it appears that the suction-force coefficient is saturated for angles of attack below 28 deg. As the angle of attack is increased, larger values of momentum coefficient are required to prevent the onset of stall. Using the active flow control with pulsed blowing, high lift can be maintained at angles of attack larger than 30 deg.

The difference between the post and prestall behaviors can clearly be seen in the plot of percentage increase in C_S (i.e., $\Delta C_S/C_S$) against angle of attack shown in Fig. 8. For the prestall incidences, the greater the momentum coefficient, the greater the percent increase in C_S, although the increase is small (less than 9%). In the poststall region, much larger increases are possible. The effect of excitation clearly becomes saturated at some minimum value of C_μ for each angle of attack. For example, at 28 deg, the effect of flow control becomes saturated between $C_\mu = 0.02$ and 0.05%. As the angle of attack increases, the minimum C_μ required to saturate the effect of flow control increases, as does the maximum percentage increase in C_S achievable. In the maximum case, a C_μ of 0.8% is required to increase C_S by 64%, which happens at an angle of attack of $\alpha = 32$ deg.

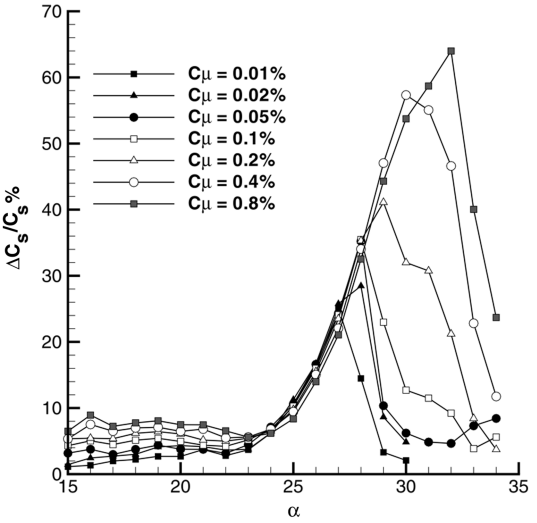

Fig. 8 Variation of percent increase in suction-force coefficient as a function of incidence; $St = 1.5$

Effectiveness is an important parameter when considering the efficiency of a flow control method. For this case, the effectiveness is defined as the ratio of change in suction-force coefficient to momentum coefficient (i.e., $\Delta C_S/C_\mu$). Pulsed blowing is more effective at lower momentum coefficients and at incidences slightly larger than the stall angle, as shown in Fig. 9. At very large incidences (past 30 deg), for which maximum increases in suction force are observed, the effectiveness is low due to the high momentum coefficients needed to maintain attached flow. Effectiveness levels of up to 2000 attained for $C_\mu = 0.01\%$ are comparable with previous findings for a $\alpha = 60$ deg wing [13]. Figure 9 also indicates that lower momentum coefficients are more effective. This is because the effect of the technique becomes saturated at a set momentum coefficient. Control of reattachment in the poststall region is orders of magnitude more effective than the steady blowing [1].

Figure 10 shows the variation of the estimated suction-force coefficient C_S as a function of incidence for two Strouhal numbers

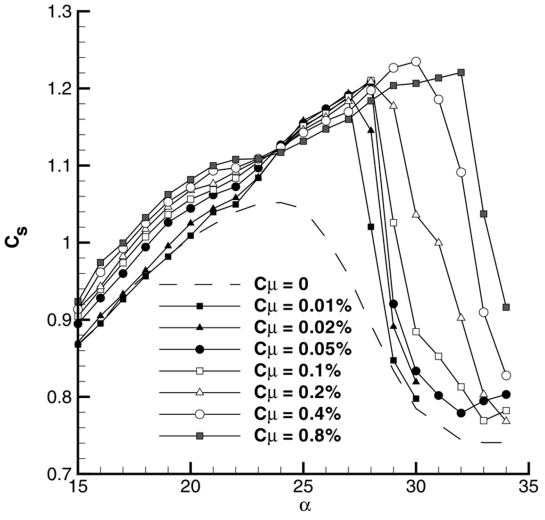

Fig. 7 Variation of suction-force coefficient as a function of angle of attack; $St = 1.5$.

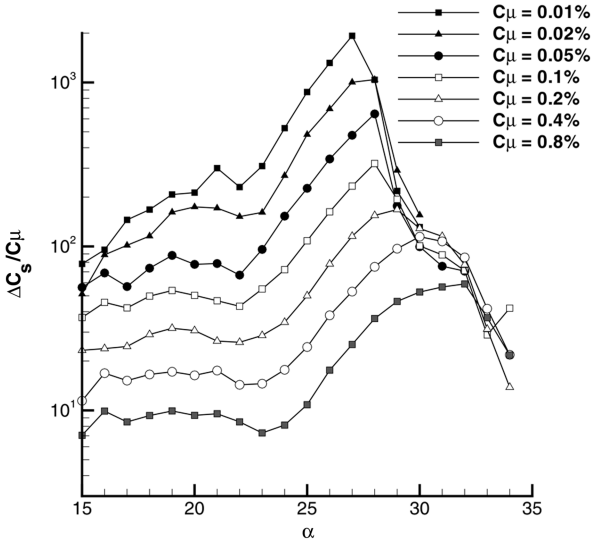

Fig. 9 Variation of effectiveness as a function of angle of attack; $St = 1.5$.

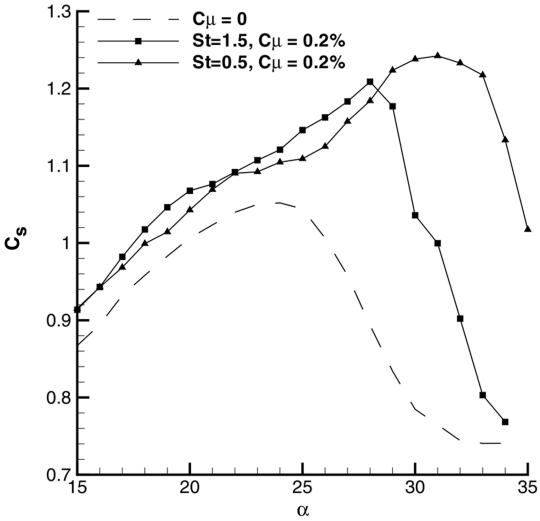

Fig. 10 Variation of suction-force coefficient as a function of incidence for $St = 0.5$ and 1.5 and $C_\mu = 0.2\%$.

($fc/U_\infty = 0.5$ and 1.5) for the same momentum coefficient of $C_\mu = 0.2\%$. Surprisingly, the lower Strouhal number was found to be more effective at very high angles of attack in the poststall region. The excitation spectrum for the $St = 0.5$ case does contain significant spectral content at $St = 1.5$, but it is clear that for $C_\mu = 0.2\%$, the lower excitation frequency is more effective. Although the optimum frequency range was found to be $St = 1$ to 2 in the oscillating-wing experiments, care should be taken in the interpretation of this result. For the oscillating wings, as the frequency is increased, the velocity of the leading edge also increases, resulting in the amplitude of excitation being proportional to the forcing frequency. In other words, at small frequencies, the amplitude is also small for the oscillating wings. In addition, the results shown in Fig. 10 might be simply due to the differences in the angle of attack; that is, the optimum frequency range might depend on the angle of attack. These aspects are being investigated with further experiments and will be the subject of the future publications.

PIV measurements were taken to understand the effect of forcing on the flowfield. The time-averaged velocity shown in Fig. 11 indicates that the wing is just near the stall at $\alpha = 25$ deg as the shear layer reaches the wing centerline. When pulsing is introduced (in this case, at $C_\mu = 0.07\%$ and $St = 1.3$), the flow reattaches to the wing and a vortex flow pattern develops. This occurs for all three stations, with the highest crossflow velocities occurring at station A

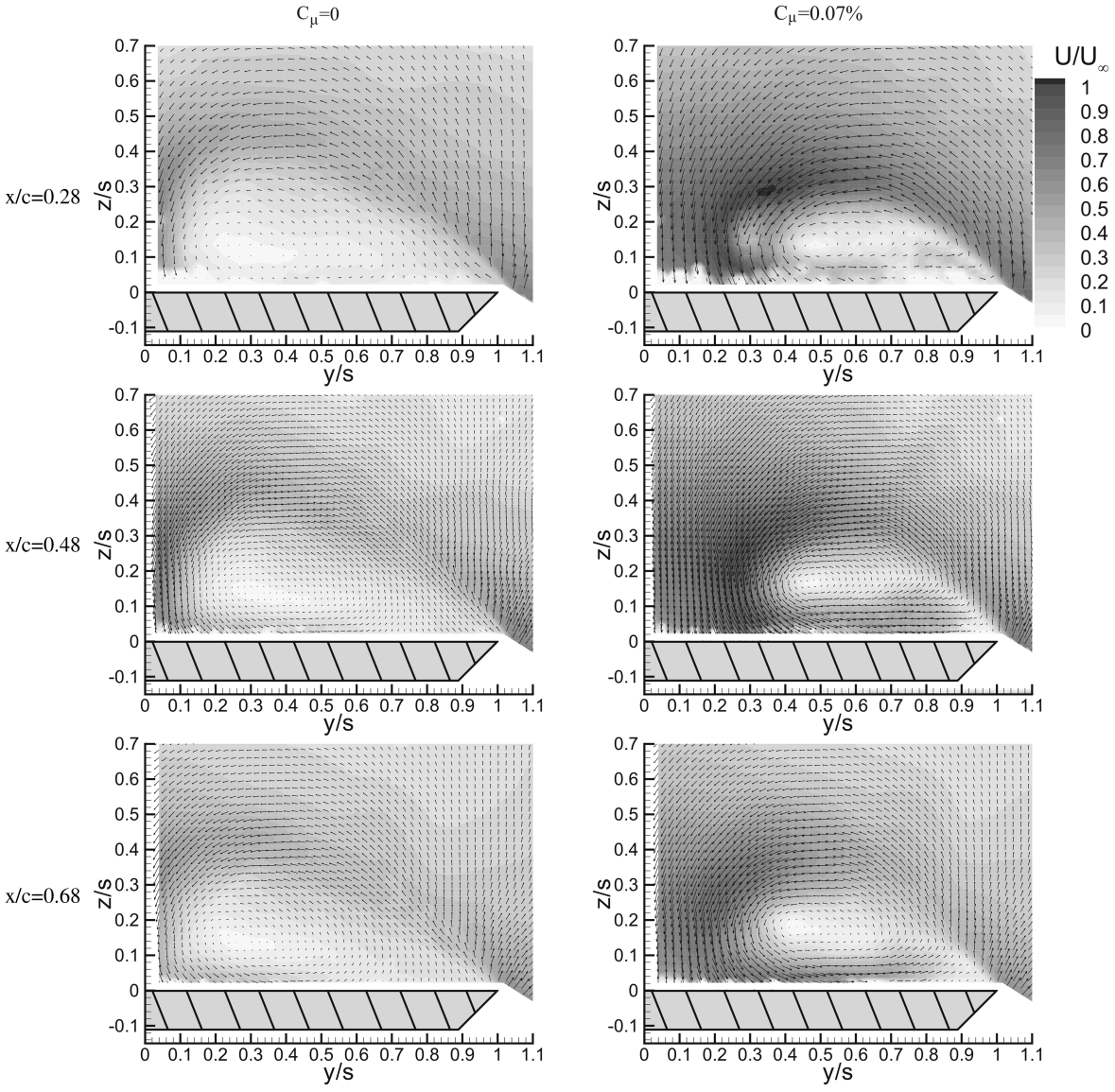

Fig. 11 Magnitude of time-averaged crossflow velocity; $\alpha = 25$ deg and $St = 1.3$.

($x/c = 0.28$) and approaching the freestream velocity in magnitude. The velocity field appears to be roughly conical, as the flow structure is similar in all three stations. High velocities occur along the shear layer as well as the reattachment region. This is confirmed by the streamlines (Fig. 12) getting closer together in these regions. The calculated streamlines from the averaged PIV measurements show distinct differences between the forced and reference (unforced) cases. At $C_\mu = 0$, a weak recirculation region is present. The location of the center of this pattern is at $y/s = 0.26$–0.33, depending on the streamwise station. An interesting point to note is that the streamlines in this case emanate outward from the center of the recirculation region. This indicates that the radial velocity in the center region is directed outward. The streamlines for the $C_\mu = 0.07\%$ case show a significantly stronger vortex flow pattern. The streamlines converge to the center of the vortex core in station B ($x/c = 0.48$). The nature of the axial flow in the core will be discussed later in the paper. With forcing, the center of the vortex flow pattern moves outboard to $y/s = 0.45$–0.53, significantly further outboard of the $C_\mu = 0$ case. This is because the flow has completely reattached and the attachment line has also moved outboard. When comparing the streamlines near the leading edge of the wing, the main difference is that for the $C_\mu = 0$ case, the streamlines leave the leading edge at an angle of approximately 45 deg, toward the centerline of the wing. By contrast, in the $C_\mu = 0.07\%$ case, the streamlines leave the wing tip almost vertically. The effect of flow control on the vortical flow is also evident from the examination of the velocity fluctuations. Normalized turbulence intensity is shown for station C ($x/c = 0.68$) in Fig. 13. The $C_\mu = 0.07\%$ case clearly shows a high level of

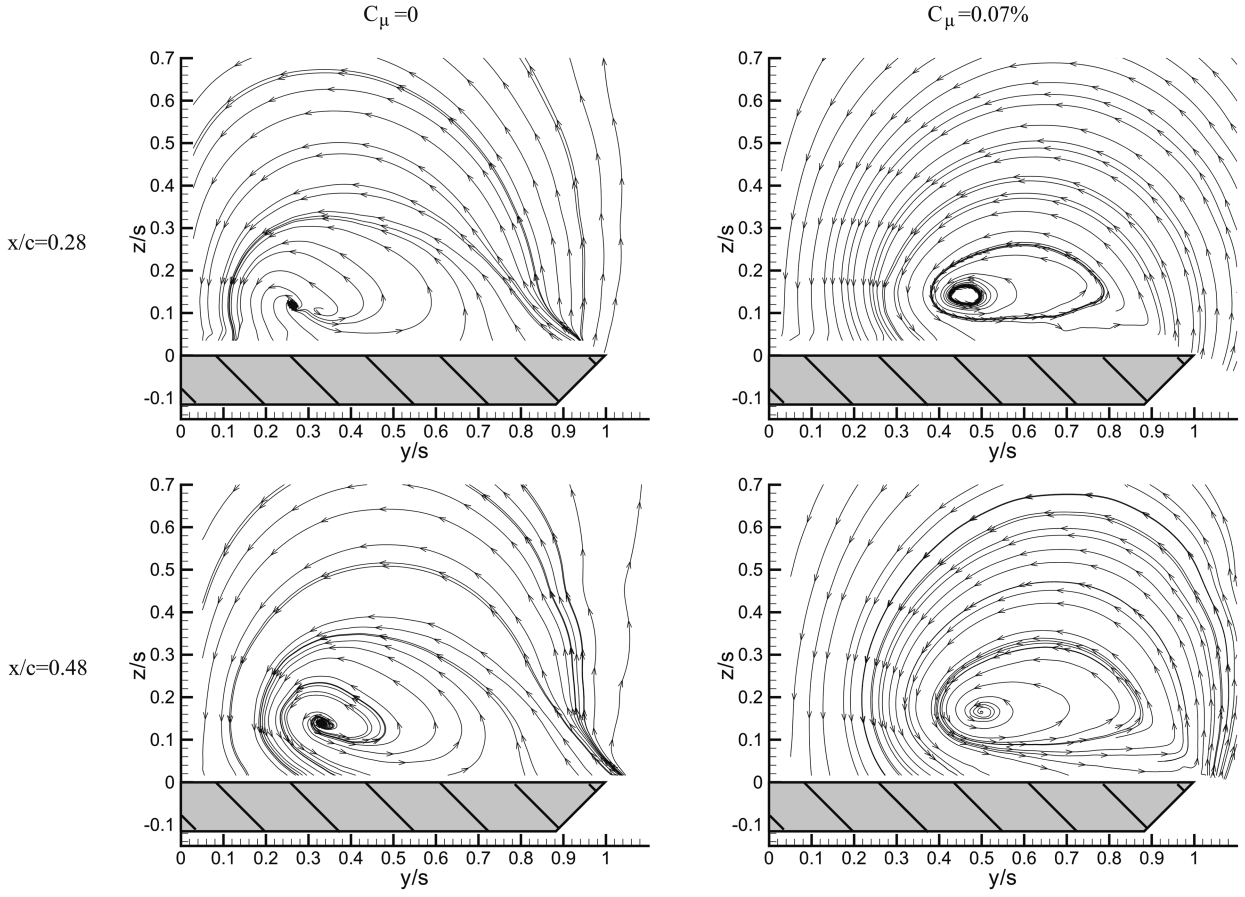

Fig. 12 Time-averaged streamline patterns in a crossflow plane; $\alpha = 25$ deg and $St = 1.3$.

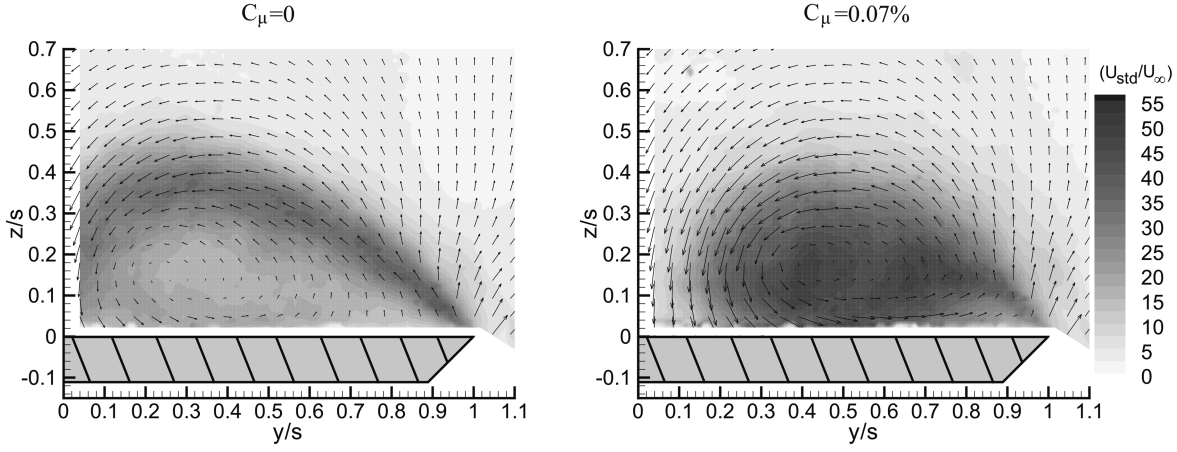

Fig. 13 Variation of turbulence intensity in a crossflow plane; $x/c = 0.68$, $\alpha = 25$ deg and $St = 1.3$.

turbulence distributed uniformly throughout the vortex, which is an indication of vortex breakdown at this station. In contrast, the $C_\mu = 0$ case shows the presence of the shear layer coming from the leading edge of the wing.

Figure 14 shows the crossflow velocity and streamlines at $x/c = 0.28$ for a larger angle of attack: $\alpha = 30$ deg. In this case, the wing is in deep stall for the reference case (no blowing), as evidenced by the velocity and the streamline pattern, which suggest that the stagnation point moves onto the wing centerline at $z/s \approx 0.8$. The streamlines appear to spiral out in the recirculation region. With forcing, the reattachment is observed with much larger crossflow velocities inboard ($y/s \approx 0.2$) and also near the wing surface. In this case, the streamlines spiral in toward the center of the vortical flow. The other features of the streamline pattern are similar to those of the lower incidence of $\alpha = 25$ deg.

The near-surface velocity measurements shown in Fig. 15 reveal a large reversed flow region on the wing surface for the no-control case. With excitation, the flow reattaches near the wing centerline, as evidenced by the streamlines becoming very close to each other and also diverging further downstream. This surface flow pattern at $\alpha = 30$ deg is similar to that of a lower incidence before stall [17].

One important aspect of the reattachment and the vortical flow established over the wing is the nature of the axial flow. This was investigated by PIV measurements in a plane through the vortex

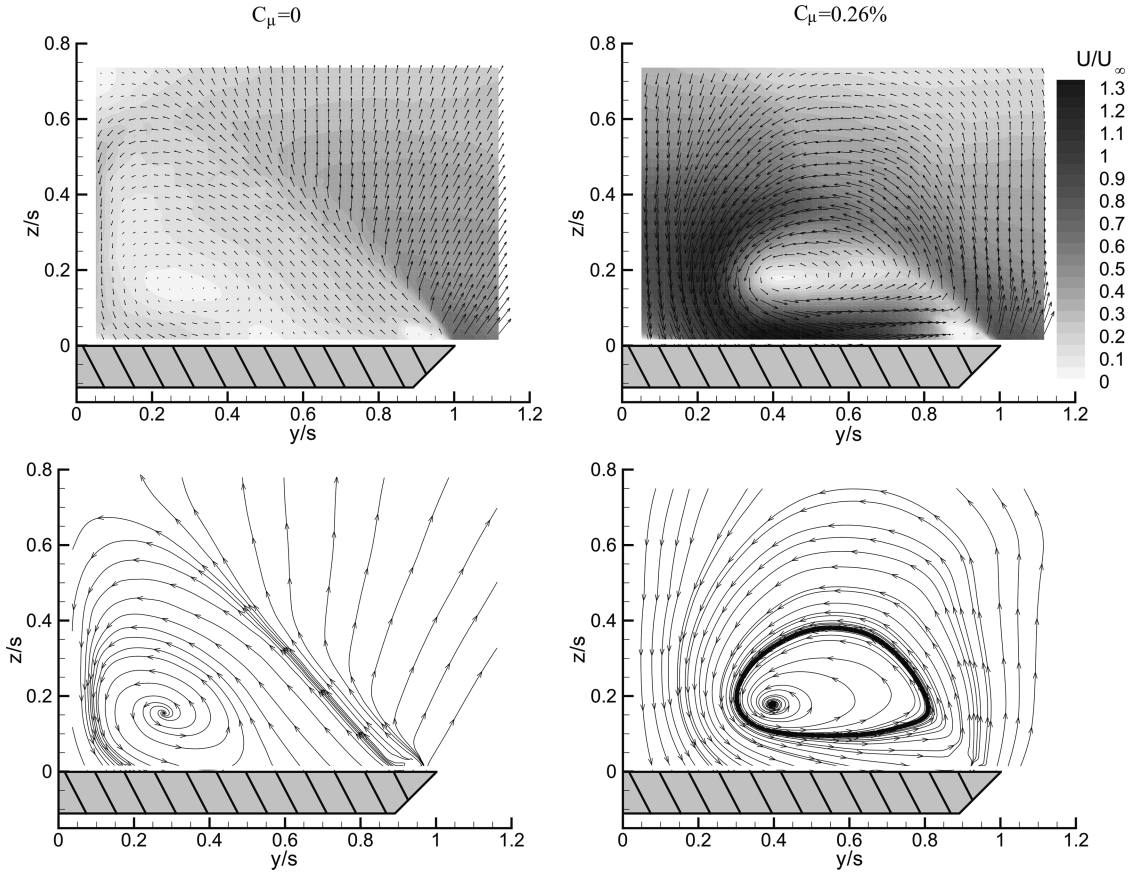

Fig. 14 Time-averaged crossflow velocity field and streamlines; $\alpha = 30$ deg, $x/c = 0.28$ and $St = 1.5$.

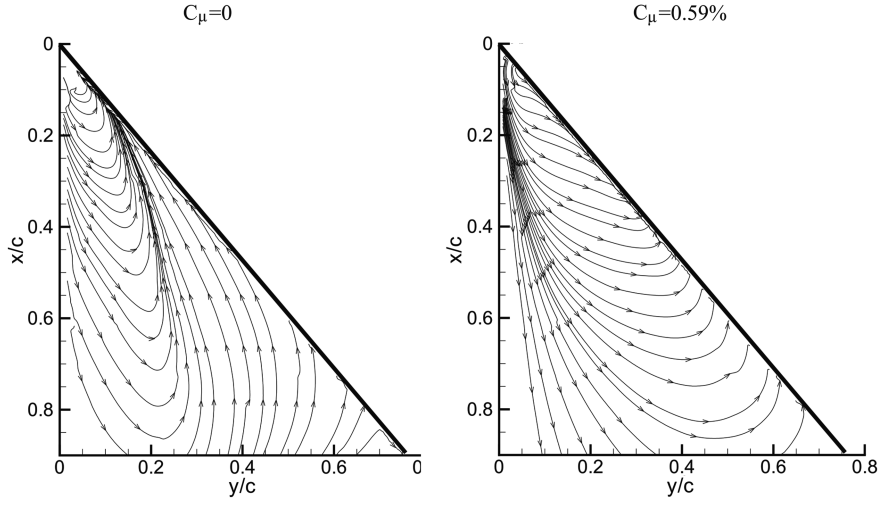

Fig. 15 Time-averaged near-surface streamlines; $\alpha = 30$ deg and $St = 1.5$.

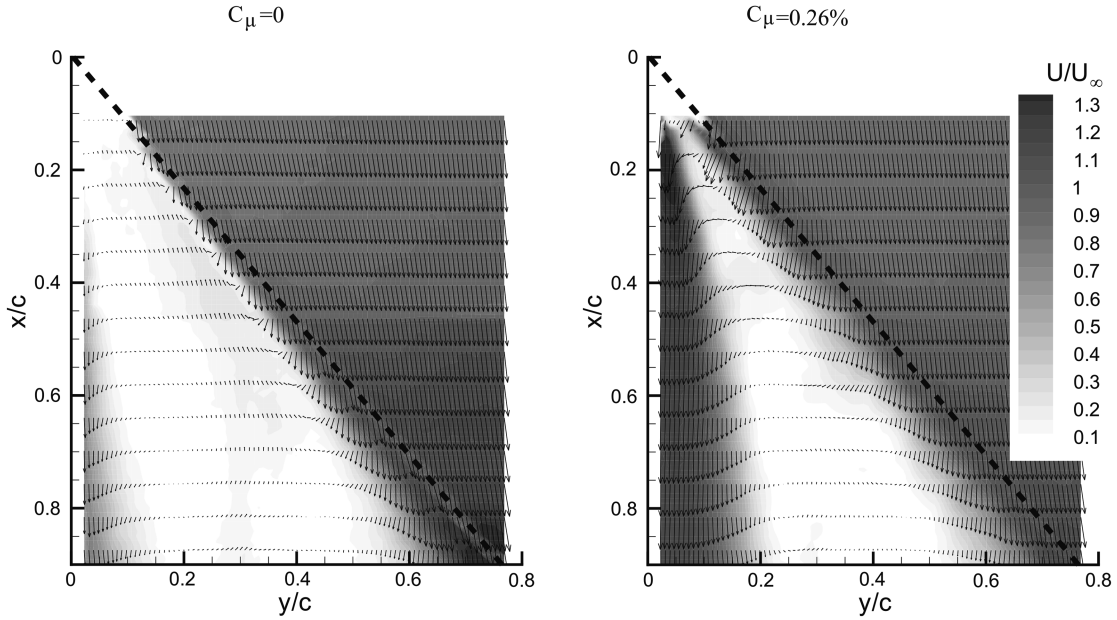

Fig. 16 Time-averaged velocity field in a plane through the vortex core; $\alpha = 30$ deg and $St = 1.5$.

core. The location of the center of the vortical flow or recirculation region was found from the crossflow measurements, then the laser sheet was placed at an angle ϕ with respect to the freestream velocity to pass through the core. This angle was the same ($\phi = 21$ deg) for $C_\mu = 0$ and 0.26%, corresponding to the cases in Fig. 14. The time-averaged velocity fields in these planes are shown in Fig. 16. It is seen that the separated region with low axial velocity or almost stagnant fluid is evident for the reference case. This massively separated region covers most of the wing, including the region near the centerline (The dashed line shows the projection of the leading edge in the measurement plane.) With active flow control, the region with low velocity is smaller, but still substantial. This indicates that there is virtually no axial flow in the vortex core in the region studied (as far as up to $x/c \approx 0.1$; accurate measurements cannot be obtained very close to the apex, due to the reflection of the laser sheet). This result confirms that vortex breakdown is at the apex or very close to the apex. Other measurements for larger momentum coefficients (not shown here) indicated that the leading-edge vortex always underwent breakdown before $x/c = 0.1$. Although delayed breakdown could be observed for the oscillating wings [3–5], the equivalent momentum coefficients are thought to be much larger than those used in present experiments.

Phase-averaged PIV measurements in a crossflow plane at $x/c = 0.48$ are shown in Fig. 17 for $\alpha = 30$ deg, $C_\mu = 0.44\%$, and $St = 1.5$. For clarity, only every third vector is plotted. The velocity field is shown at different phases of the pulsing cycle, with the duty cycle at 20%. The blowing starts at $t/T = 0$ and ends around $t/T = 0.20$. A small vortex is generated with pulsed blowing, which travels along the shear layer and interacts with the recirculation region. The apparent center of the large vortical region moves inboard and away from the surface ($0.20 \leq t/T \leq 0.40$), then outboard and closer to the surface ($0.50 \leq t/T \leq 0.80$). The interaction of the perturbation, due to blowing, with the mean flow (also shown in Fig. 17) causes a cyclic variation of the location of the large vortical region. This apparent displacement of the vortex and subsequent relaxation also has an effect on the reattachment region and high crossflow velocities observed away from the leading edge. Following the introduction of the perturbation, the region of large velocity travels along the shear layer, reaches $y/s \approx 0.2$ for $t/T = 0.50$, causing very large (and almost parallel) velocities near the wing surface, before the whole flowfield relaxes back to the mean flow at $t/T = 0.80$.

Experiments were also conducted for pulsed blowing from a finite length slot, rather than the whole length along the leading edge. This kind of partial (or distributed) blowing may be more realistic for practical applications. Various slot lengths were investigated in preliminary experiments. It was found that blowing from the entire slot length still produces the largest attainable increase in suction force for large momentum coefficients. However, blowing from a smaller section of the leading edge can be more effective at low momentum coefficients. Figure 18 shows the increase in the suction force as a function of momentum coefficient for various active slot locations. For all cases, the length of the slot was 25% of the total length of the leading edge, whereas the location of the blowing slot was varied systematically. The inset shows the location of the slot for each case. As a reference, the case of blowing from the entire slot is shown with dashed lines. It is evident that for some finite span slot locations, partial blowing is more effective than blowing from the entire leading edge: in particular, at low momentum coefficients. This is particularly clear if the slot is located in the forward half of the wing (but not starting from the apex). As the wing was completely stalled for the reference (no-blowing) case, the effective location of blowing is not related to the vortex breakdown phenomenon.

For one particularly promising case for which significant lift enhancement can be achieved at very small momentum coefficients, the pressure distribution at $x/c = 0.28$ is shown with that of blowing from the entire length of the slot at $\alpha = 30$ deg in Fig. 19. The measurement station ($x/c = 0.28$) is just at the beginning of the blowing section (from $x/c = 0.25$ to 0.50). For partial blowing, the generation of a pressure-profile characteristic of vortex lift for $C_\mu \geq 0.13\%$ indicates that partially reattached flow may already be established upstream of the blowing region.

IV. Conclusions

Active flow control on a nonslender delta wing with a sweep angle of $\alpha = 50$ deg at poststall incidences was demonstrated by pulsed blowing from the leading edge. Pressure and velocity measurements were made to document the effect of unsteady excitation. For poststall incidences, a flat pressure distribution, characteristic of stalled flow, changes to a pressure distribution with a strong suction peak, indicating the formation of a vortex, when the separated shear layer is excited at a frequency corresponding to $St = 1.5$. The estimated suction-force coefficient increases significantly for momentum coefficients as low as 0.01%. Once the complete reattachment of the shear layer is reached, further increases in momentum coefficient do not improve the pressure distribution. As

the angle of attack is increased, the minimum C_μ required to saturate the flow control (to produce complete reattachment) increases, as does the maximum increase in the suction force. Stall can be delayed by up to 8 deg for $C_\mu = 0.8\%$. Maximum values of the effectiveness factor $\Delta C_S/C_\mu$ are comparable with that of a more slender delta wing with $\Lambda = 60$ deg. A lower Strouhal number ($St = 0.5$) was found to be more effective at very high angles of attack and delayed stall further, when compared with $St = 1.5$.

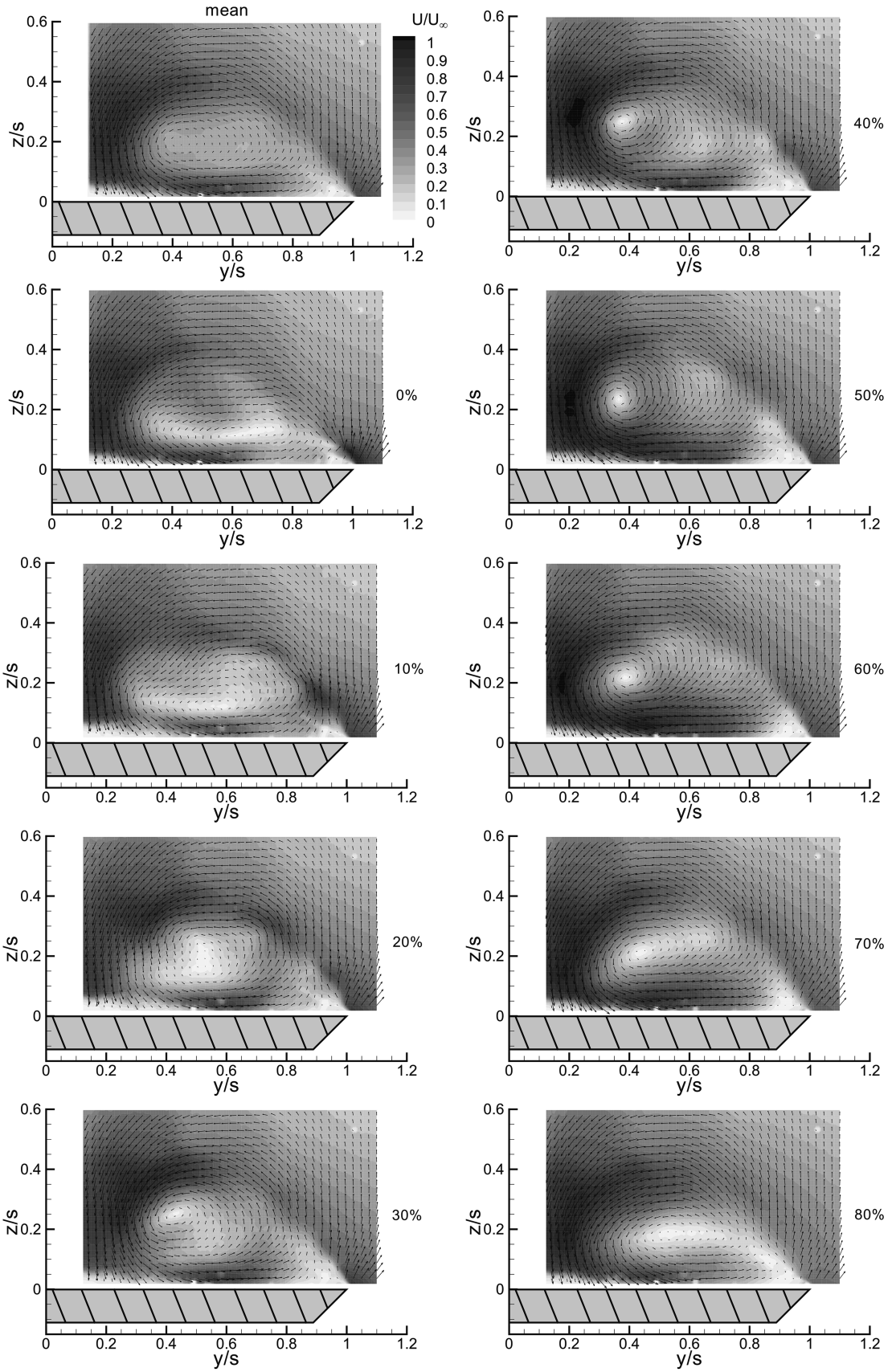

Fig. 17 Magnitude of phase-averaged crossflow velocity; $x/c = 0.48$, $\alpha = 30$ deg, $C_\mu = 0.44\%$ and $St = 1.5$.

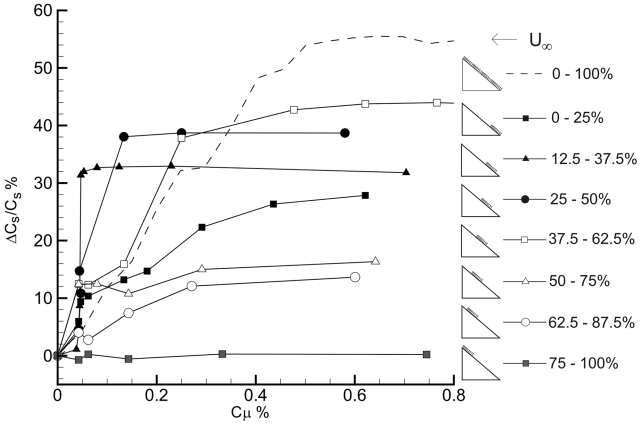

Fig. 18 Variation of percent increase in suction-force coefficient as a function of momentum coefficient for various slot locations; $\alpha = 30$ deg and $St = 1.5$.

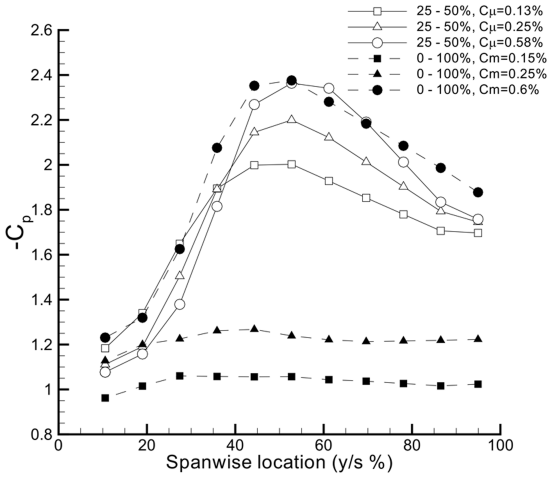

Fig. 19 Spanwise pressure distribution at $x/c = 0.28$ for partial blowing between 25 and 50% of the leading edge; $\alpha = 30$ deg and $St = 1.5$.

For an angle of attack near stall, velocity measurements show that flow reattachment is promoted with forcing, and a vortex flow pattern develops. The time-averaged location of the center of the vortical region moves outboard with excitation. Similar results were obtained for even higher angles of attack in the deep-stall region. The near-surface flow pattern obtained from the PIV measurements clearly shows reattachment in the forward part of the wing. There is no jetlike axial flow in the core of the vortex, which confirms that there is breakdown at or very near the apex. Phase-averaged measurements reveal the perturbation due to the pulsed blowing, its interaction with the shear layer and vortex, apparent displacement of the vortex core, and relaxation of the reattachment region over a cycle.

Experiments with distributed (3-D) forcing from finite span slots show that partial blowing may be more effective at low momentum coefficients. In particular, slots located in the forward half of the wing were found to be more effective. Flow reattachment upstream of the slot appears to be possible, as evidenced by the pressure profile that is characteristic of a leading-edge vortex.

Acknowledgments

The authors would like to acknowledge funding from the Overseas Research Award Scheme and the Research Councils United Kingdom Academic Fellowship in Unmanned Air Vehicles.

References

[1] Gursul, I., Wang, Z., and Vardaki, E., "Review of Flow Control Mechanisms of Leading edge Vortices," *Progress in Aerospace Sciences*, Vol. 43, Nos. 7–8, Oct.–Nov. 2007, pp. 246–270. doi:10.1016/j.paerosci.2007.08.001

[2] Yaniktepe, B., and Rockwell, D., "Flow Structure on a Delta Wing of Low Sweep Angle," *AIAA Journal*, Vol. 42, No. 3, 2004, pp. 513–523. doi:10.2514/1.1207

[3] Vardaki, E., Gursul, I., and Taylor, G., "Physical Mechanisms of Lift Enhancement for Flexible Delta Wings," 43rd Aerospace Sciences Meeting and Exhibit AIAA Paper 2005-0867, Reno, NV, Jan. 2005.

[4] Gursul, I., Vardaki, E., and Wang, Z., "Active and Passive Control of Reattachment on Various Low-Sweep Wings," 44th AIAA Aerospace Sciences Meeting and Exhibit AIAA Paper 2006-506, Reno, NV, Jan. 2006.

[5] Vardaki, E., Wang, Z., and Gursul, I., "Flow Reattachment and Vortex Re-Formation on Oscillating Low Aspect Ratio Wings," *AIAA Journal*, Vol. 46, No. 6, 2008, pp. 1453–1462. doi:10.2514/1.32233

[6] Taylor, G. S., and Gursul, I., "Lift Enhancement over a Flexible Low Sweep Delta Wing," 2nd AIAA Flow Control Conference AIAA 2004-2618, Portland, OR, 2004.

[7] Taylor, G. S., Kroker, A., and Gursul, I., "Passive Flow Control over Flexible Nonslender Delta Wings," 43rd Aerospace Sciences Meeting and Exhibit AIAA Paper 2005-0865, Reno, NV, Jan. 2005.

[8] Taylor, G., Wang, Z., Vardaki, E., and Gursul, I., "Lift Enhancement over Flexible Nonslender Delta Wings," *AIAA Journal*, Vol. 45, No. 12, 2007, pp. 2979–2993. doi:10.2514/1.31308

[9] Roos, F. W., and Kegelman, J. T., "Control of Coherent Structures in Reattaching Laminar and Turbulent Shear Layers," *AIAA Journal*, Vol. 24, No. 12, 1986, pp. 1956–1963. doi:10.2514/3.9553

[10] Gursul, I., Gordnier, R., and Visbal, M., "Unsteady Aerodynamics of Nonslender Delta Wings," *Progress in Aerospace Sciences*, Vol. 41, No. 7, Oct. 2005, pp. 515–557. doi:10.1016/j.paerosci.2005.09.002

[11] Gordnier, R. E., and Visbal, M. R., "Compact Differences Scheme Applied to Simulation of Low-Sweep Delta Wing Flow," *AIAA Journal*, Vol. 43, No. 8, 2005, pp. 1744–1752. doi:10.2514/1.5403

[12] Gad-el-Hak, M., and Blackwelder, R. F., "Control of the Discrete Vortices from a Delta Wing," *AIAA Journal*, Vol. 25, No. 8, 1987, pp. 1042–1049. doi:10.2514/3.9740

[13] Margalit, S., Greenblatt, D., Seifert, A., and Wygnanski, I., "Delta Wing Stall and Roll Control Using Segmented Piezoelectric Fluidic Actuators," *Journal of Aircraft*, Vol. 42, No. 3, 2005, pp. 698–709. doi:10.2514/1.6904

[14] Rullan, J., Vlachos, P. P., and Telionis, D. P., "Aerodynamics and Flow Control over Swept Wings and Wings with Diamond Planform," 45th AIAA Aerospace Sciences Meeting and Exhibit, Reno, NV, AIAA Paper 2007-0879, Jan. 2007.

[15] Margaris, P., "Wing Tip Votex Control by means of Tip Blowing," Ph.D. Thesis, Mechanical Engineering Dept., Univ. of Bath, Bath, England, U.K., 2006.

[16] Attar, P. J., Gordnier, R. E., and Visbal, M. R., "Numerical Simulation of the Buffet of a Full Span Delta Wing at High Angle of Attack," 47th AIAA/ASME/ASCE/AHS/ASC Structures, Structural Dynamics, and Materials Conference AIAA Paper 2006-2075, Newport, RI, May 2006.

[17] Taylor, G. S., and Gursul, I., "Buffeting Flows over a Low-Sweep Delta Wing," *AIAA Journal*, Vol. 42, No. 9, 2004, pp. 1737–1745. doi:10.2514/1.5391